IOP Publishing Measurement Science and Technology
Meas. Sci. Technol. **31** (2020) 055104 (14pp) https://doi.org/10.1088/1361-6501/ab6674

# Non-damping system reset algorithm for shipborne grid strap-down inertial navigation systems

**Tao Fang**[1], **Weiquan Huang**[1], **Alan F Lynch**[2] **and Zongyi Wang**[1]

[1] College of Automation, Harbin Engineering University, Harbin 150001, People's Republic of China
[2] Department of Electrical and Computer Engineering, University of Alberta, Edmonton, AB T6G 1H9, Canada

E-mail: huangweiquan@hrbeu.edu.cn

Received 1 November 2019, revised 12 December 2019
Accepted for publication 31 December 2019
Published 26 February 2020

**Abstract**

The system reset algorithms realized in damping state rely heavily on the output of Doppler velocity logs (DVLs). Aiming at a shipborne grid strap-down inertial navigation system (SGSINS), this paper addresses a non-damping system reset algorithm to estimate the gyroscope drifts. First, the SGSINS is integrated with the DVL to estimate the horizontal attitude errors, and the estimation results are introduced to the system reset. Next, to ensure the $\boldsymbol{P}$ equation can be utilized to design the non-damping system reset scheme, the $\boldsymbol{P}$ equation is reformulated by reserving the horizontal attitude errors as the correction terms. Finally, with the assistance of two intermittent or short continuous external yaw and position, the two-point and optimum system reset schemes are designed based on the $\boldsymbol{P}$ equation and $\psi$ equation. Simulation results indicate the algorithm can estimate the gyroscope drifts accurately in non-damping state. Compensating the gyroscope drifts can efficiently suppress the drifted errors in SGSINS. Because it takes a short time to estimate the horizontal attitude errors, compared with the existing algorithms realized in damping state, the proposed algorithm greatly shortens the time of using DVL, and this improves the reliability of the algorithm in practical application.

Keywords: system reset, Doppler velocity log, shipborne grid strap-down inertial navigation system, non-damping, gyroscope drifts

(Some figures may appear in colour only in the online journal)

## 1. Introduction

The strap-down inertial navigation system (SINS) is taken as the core navigation system in the field of ship navigation [1–3]. The north-pointing SINS mechanization is widely applied in the non-polar region; however, it has difficulty calculating the accurate yaw and longitude in the polar region. It has been proved that the grid SINS mechanization is feasible to be applied in the polar region [4–7]. Since SINS is a dead reckoning system, the error deteriorates with time in grid SINS [8, 9], and the gyroscope drift is the primary error source. For a long-term shipborne grid strap-down inertial navigation system (SGSINS), specific techniques must be implemented to suppress the deteriorated errors.

In view of keeping the navigation autonomy of the ship, the system reset is taken as an effective method to suppress the navigation errors as well as extend the navigation time of SGSINS. The system reset aims to reset the system errors and compensate the gyroscope drifts under the assistance of intermittent or short continuous external navigation information [10, 11]. Under the assistance of intermittent external navigation information, aiming at a platform inertial navigation system, [12] introduced two-point and three-point system reset schemes, thereinto the two-point system reset scheme can also be applied to SINS. Aiming at SINS, [13] designed the progressive two-point system reset scheme, where the inertial frame is introduced to replace the *OEPQ* frame. The scheme eliminates the constraints in [12] that the latitude and

 

attitude of the ship are not allowed to change in the system reset. Similarly, [14] designed the progressive three-point system reset scheme; however, due to the coupling effect between the horizontal gyroscope drifts and yaw error, only Z-axis gyroscope drift could be estimated. According to the error propagation rule of the azimuth damping INS, [15] designed the corresponding system reset scheme. Aiming at a transversal SINS mechanization working in the polar region, on the basis of [14], [16] designed the three-point system reset scheme, and the scheme obtained identical simulation results to [14]. Aiming at SGSINS, [17] derived the $\boldsymbol{P}$ equation and designed the two-point and three-point system reset schemes based on the inertial frame. The system reset algorithms mentioned above should be realized in damping state. In order to eliminate this constraint, [18] proposed a non-damping system reset algorithm. In [18], SINS is integrated with external velocity and position to estimate the horizontal attitude errors. In order to ensure the two-point system reset scheme can be realized in the non-damping state, the horizontal attitude errors are compensated through feedback calibration by using the estimation results from the Kalman filter. Note that the feedback calibration to restrain the horizontal attitude errors is the novel damping method that was introduced in [19], and this method relies heavily on the initial parameters of the filter, which is difficult to implement in practical application. With the assistance of short continuous external yaw and position, [20] proposed an optimum system reset scheme based on the inertial frame, and the gyroscope drifts are estimated by Kalman filter. Note that the scheme should be realized in damping state. Under the assistance of continuous external position, [21] proposed a non-damping optimum system reset algorithm to estimate the gyroscope drifts. However, the gyroscope drift in the east direction cannot be estimated through the algorithm.

The $\boldsymbol{P}$ equation and the $\boldsymbol{\psi}$ equation are the key in designing the system reset scheme. The $\boldsymbol{P}$ equation relates the position errors to the vector angle $\boldsymbol{\psi}$ and yaw error, and the $\boldsymbol{\psi}$ equation relates the vector angle $\boldsymbol{\psi}$ to the gyroscope drifts. In the previous research, the $\boldsymbol{P}$ equation was derived based on the assumption that the horizontal attitude errors are approximately zero [12–14, 16, 17]. To ensure horizontal attitude errors can be approximated to zero, the SINS needs to work in damping state in the system reset. In this way, the estimation accuracy of the gyroscope drift relies heavily on the damping performance. The Doppler velocity log (DVL) is usually used to dampen the errors of the SINS; however, the accuracy of the DVL is extremely vulnerable to the ocean current and the maneuvering of the ship [22–24]. The working state of the SINS frequently switches between damping state and non-damping state based on the availability of the DVL. When the working state switches in the system reset, the error propagation rule of damping SINS breaks [25], and the estimation accuracy of gyroscope drift degrades.

With the aim of solving the problem mentioned above, this paper addresses a non-damping system reset algorithm for the SGSINS. First, on the basis of the SGSINS error model, the SGSINS is integrated with the DVL to estimate the horizontal attitude errors, and the estimation results are introduced to the system reset. Next, in order to ensure the system reset algorithm can be realized in non-damping state, we reformulated the $\boldsymbol{P}$ equation. Different from the $\boldsymbol{P}$ equation in [17], the horizontal attitude errors are contained as the correction terms in $\boldsymbol{P}$ equation which aims to eliminate the approximate error caused by ignoring the horizontal attitude errors. Finally, under the assistance of two intermittent or short continuous external yaw and position, we designed the two-point and optimum system reset schemes, respectively. The simulation tests demonstrate that the designed system reset schemes can estimate the gyroscope drifts in non-damping state accurately. Compensating the gyroscope drifts can efficiently restrain the drifted errors in the SGSINS. Because it only takes a short time to estimate the horizontal attitude errors in the system reset, compared with the existing system reset algorithms realized in damping state, the proposed algorithm greatly shortens the time of using DVL, which improves the reliability of the algorithm in practical application.

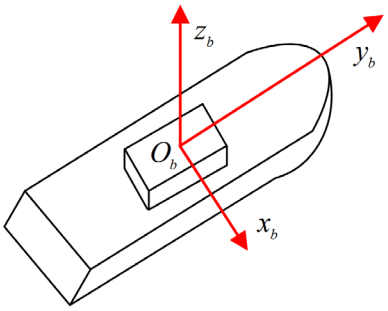


**Figure 1.** The body frame $b$.

The paper is organized as follows: section 2 introduces the relevant coordinate systems and SGSINS error model; section 3 reformulates the $\boldsymbol{P}$ equation, and the $\boldsymbol{\psi}$ equation is also introduced; under the assistance of two intermittent or short continuous external yaw and position, the two-point and optimum system reset schemes are designed in sections 4, and 5 validates the effectiveness of the proposed system reset schemes; section 6 gives the conclusions.

## 2. Coordinate systems and SGSINS error model

### *2.1. The relevant coordinate systems*

The coordinate systems used in this paper include the following.

Body frame $b$: the body frame has its origin at the center of mass of the ship. The pitch axis $x_b$, roll axis $y_b$ and yaw axis $z_b$ point to the right-hand side, forward and upward, respectively. The body frame is shown in figure 1:

Earth-fixed frame $e$: the earth-fixed frame has its origin at the center of mass of the earth. $x_e$ lies along the intersection line of the equatorial plane and Greenwich meridian; $y_e$ lies in the equatorial plane and is perpendicular to $x_e$; $z_e$ coincides with the polar axis. $x_e$, $y_e$ and $z_e$ constitute the right-handed coordinate system.

Inertial frame $i$: the inertial frame has its origin at the center of mass of the earth. $x_i$ lies in the equatorial plane and points to a fixed star; $y_i$ lies in the equatorial plane and is perpendicular

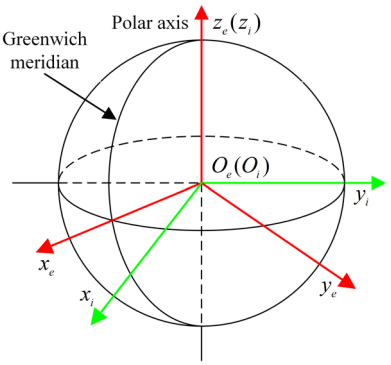


**Figure 2.** The inertial frame $i$ and earth-fixed frame $e$.

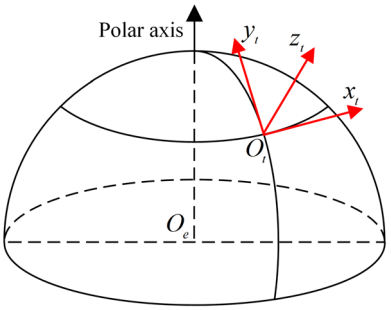


**Figure 3.** The geographic frame $t$.

to $x_i$; $z_i$ coincides with the polar axis. $x_i$, $y_i$ and $z_i$ constitute the right-handed coordinate system. The inertial frame and earth-fixed frame are illustrated in figure 2:

Geographic frame $t$: the geographic frame has its origin at the center of mass of the ship. $x_t$ lies in the local horizontal plane and points to the east; $y_t$ lies in the local horizontal plane and points to the north; $z_t$ is perpendicular to the local horizontal plane and points upward. $x_t$, $y_t$ and $z_t$ constitute the right-handed coordinate system. The geographic frame is drawn in figure 3:

*OEPQ* frame: the *OEPQ* frame has its origin at the center of mass of the ship. *OE* is tangent to the latitude circle and points to the east; *OP* is parallel to the polar axis and points to the north; *OQ* lies in the latitude circle and is perpendicular to the polar axis. *OE*, *OP* and *OQ* constitute the right-handed coordinate system. The *OEPQ* frame is shown in figure 4:

Grid frame $G$: the grid frame is chosen as the navigation frame for SGSINS. The grid frame has its origin at the center of mass of the ship. $y_G$ points to the north, meanwhile $y_G$ is parallel to the Greenwich meridian and lies in the local horizontal plane; $x_G$ points to the east, meanwhile $x_G$ lies in the local horizontal plane and is perpendicular to $y_G$; $z_G$ coincides with $z_t$. $x_G$, $y_G$ and $z_G$ constitute the right-handed coordinate system.

Mathematical platform frame $p$: $p$ imitates $G$, and the origin coincides with the origin of $G$. The vector angle between $G$ and $p$ is defined as $\boldsymbol{\phi}$, which is usually called the grid attitude error angle.

Computer frame $c$: $c$ imitates $G$, and the origin is the position calculated by SGSINS. The vector angle between $G$ and $c$ is defined as $\delta\boldsymbol{\theta}$, and the vector angle between $p$ and $c$ is defined as $\boldsymbol{\psi}$. $\boldsymbol{\phi}$, $\delta\boldsymbol{\theta}$ and $\boldsymbol{\psi}$ satisfy:

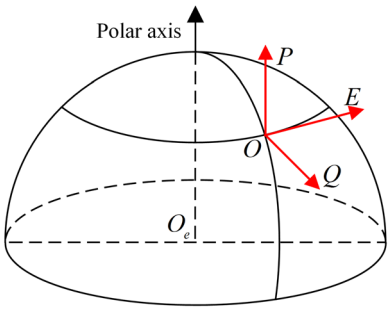


**Figure 4.** The *OEPQ* frame.

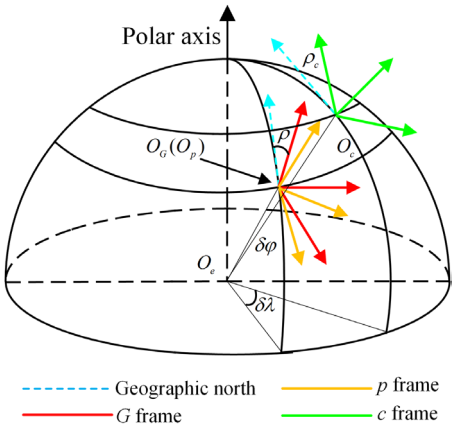


**Figure 5.** The grid frame, mathematical platform frame and computer frame.

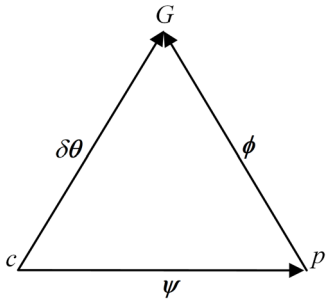


**Figure 6.** The relationship between $\boldsymbol{\phi}$, $\delta\boldsymbol{\theta}$ and $\boldsymbol{\psi}$.

$$\boldsymbol{\phi} = \delta\boldsymbol{\theta} + \boldsymbol{\psi}. \tag{1}$$

The grid frame, mathematical platform frame and computer frame are illustrated in figure 5. In figure 5, $\delta\lambda$ and $\delta\varphi$ denote the longitude and latitude errors; $\rho$ and $\rho_c$ denote the true grid azimuth and the calculated grid azimuth outputted by SGSINS.

The relationship between $\boldsymbol{\phi}$, $\delta\boldsymbol{\theta}$ and $\boldsymbol{\psi}$ is illustrated in figure 6.

The definitions of the abovementioned coordinate systems can refer to [8, 19]. The proposed system reset algorithm is performed upon the SGSINS mechanization. [19] has given a detailed description of the SGSINS mechanization.

### 2.2. SGSINS error model

In order to eliminate the approximate error caused by ignoring the horizontal attitude errors in deriving the $\boldsymbol{P}$ equation, the SGSINS is integrated with the DVL to estimate

the horizontal attitude errors, and the estimation results are introduced to the system reset. The vertical velocity is negligible in shipborne application. Defining the state vector as $\boldsymbol{x} = \begin{bmatrix}\phi_E^G & \phi_N^G & \phi_U^G & \delta V_E^G & \delta V_N^G & \delta X & \delta Y & \delta Z\end{bmatrix}^{\mathrm{T}}$, thereinto $\phi_E^G$, $\phi_N^G$ and $\phi_U^G$ denote the pitch, roll and grid yaw errors; $\delta V_E^G$ and $\delta V_N^G$ denote the grid east and grid north velocity errors; $\delta X$, $\delta Y$ and $\delta Z$ denote the position errors in the earth-fixed frame. The continuous-time linear process equation is formulated as

$$\dot{\boldsymbol{x}}(t) = \boldsymbol{A}(t)\boldsymbol{x}(t) + \boldsymbol{B}(t)\boldsymbol{w}(t) \tag{2}$$

where $\boldsymbol{w}(t) = \begin{bmatrix}\boldsymbol{\varepsilon}^b & \boldsymbol{\nabla}^b(1:2)\end{bmatrix}^{\mathrm{T}}$ is the process noise. $\boldsymbol{\varepsilon}^b$ denotes the gyroscope drift in the body frame; $\boldsymbol{\nabla}^b(1:2)$ denotes the first two elements of accelerometer bias $\boldsymbol{\nabla}^b$ in the body frame. The state transition matrix $\boldsymbol{A}(t)$ and the process noise matrix $\boldsymbol{B}(t)$ are obtained as follows:

$$\boldsymbol{A}(t) = \begin{bmatrix}\boldsymbol{A}_{11} & \boldsymbol{A}_{12} & \boldsymbol{A}_{13}\\ \boldsymbol{A}_{21} & \boldsymbol{A}_{22} & \boldsymbol{A}_{23}\\ \boldsymbol{A}_{31} & \boldsymbol{A}_{32} & \boldsymbol{A}_{33}\end{bmatrix}. \tag{3}$$

$$\boldsymbol{B}(t) = \begin{bmatrix}-\boldsymbol{C}_b^G & \boldsymbol{0}_{3\times 2}\\ \boldsymbol{0}_{2\times 3} & (\boldsymbol{C}_b^G)_{2|2}\\ \boldsymbol{0}_{3\times 3} & \boldsymbol{0}_{3\times 2}\end{bmatrix} \tag{4}$$

where $\boldsymbol{A}_{11} = -\boldsymbol{\omega}_{iG}^G\times$, $\boldsymbol{A}_{12} = (\boldsymbol{C}_{AV})_{3|2}$, $\boldsymbol{A}_{13} = \boldsymbol{C}_{AR1} + \boldsymbol{C}_{AR2}$, $\boldsymbol{A}_{21} = (\boldsymbol{f}^G\times)_{2|3}$, $\boldsymbol{A}_{22} = [\boldsymbol{V}^G \times \boldsymbol{C}_{AV} - (2\boldsymbol{\omega}_{ie}^G + \boldsymbol{\omega}_{eG}^G)\times]_{2|2}$, $\boldsymbol{A}_{23} = [\boldsymbol{V}^G \times (\boldsymbol{C}_{AR1} + 2\boldsymbol{C}_{AR2})]_{2|3}$, $\boldsymbol{A}_{31} = \boldsymbol{0}_{3\times 3}$, $\boldsymbol{A}_{32} = (\boldsymbol{C}_G^e)_{3|2}$ and $\boldsymbol{A}_{33} = -\boldsymbol{C}_G^e(\boldsymbol{V}^G\times)\boldsymbol{C}_R$.

The definitions of the symbols in (3) and (4) are expressed as follows:

$\boldsymbol{\omega}_{\beta\alpha}^{\gamma}$: rotation angular rate of $\alpha$ frame with respect to $\beta$ frame in $\gamma$ frame, e.g. $\boldsymbol{\omega}_{iG}^G$, $\boldsymbol{\omega}_{ie}^G$ and $\boldsymbol{\omega}_{eG}^G$;

$\boldsymbol{\Theta}\times$: the antisymmetric matrix related to $\boldsymbol{\Theta}$, e.g. $\boldsymbol{\omega}_{iG}^G\times$, $\boldsymbol{f}^G\times$, $\boldsymbol{V}^G\times$ and $(2\boldsymbol{\omega}_{ie}^G + \boldsymbol{\omega}_{eG}^G)\times$;

$(\cdot)_{m|n}$: the first $n$ columns and $m$ rows of the matrix;

$\boldsymbol{f}^G$: the accelerometer output in grid frame;

$\boldsymbol{V}^G$: velocity in grid frame;

$\boldsymbol{C}_{\text{frame1}}^{\text{frame2}}$: direction cosine matrix between frame 1 and frame 2, e.g. $\boldsymbol{C}_G^e$ and $\boldsymbol{C}_b^G$.

The detailed expressions of matrixes $\boldsymbol{C}_{AV}$, $\boldsymbol{C}_{AR1}$, $\boldsymbol{C}_{AR2}$ and $\boldsymbol{C}_R$ are formulated in the appendix.

In this paper, SGSINS and DVL are integrated through the loosely coupled method. Thereby, the difference between the velocities provided by SGSINS and DVL is taken as the measurement. The measurement equation is formulated as follows:

$$\boldsymbol{z}(t) = \begin{bmatrix}\delta V_E^G\\ \delta V_N^G\end{bmatrix} = \boldsymbol{H}\boldsymbol{x}(t) + \boldsymbol{\eta}(t). \tag{5}$$

where $\boldsymbol{z}$ is the measurement vector; the measurement matrix $\boldsymbol{H} = \begin{bmatrix}\boldsymbol{0}_{2\times 3} & \boldsymbol{I}_{2\times 2} & \boldsymbol{0}_{2\times 3}\end{bmatrix}$, and $\boldsymbol{I}_{2\times 2}$ is the $2\times 2$ identity matrix.

Note that in order to reduce the time of using DVL and improve the reliability of the system reset algorithm, we only integrate the SGSINS and DVL for a short period of time in the system reset. In section 4, figures 8 and 10 have shown the time of introducing DVL to the two-point and optimum system reset schemes.

## 3. The $\psi$ equation and the derivation of the modified *P* equation

In the field of ship navigation, the celestial navigation system (CNS) is usually taken as the yaw reference, and the global positioning system (GPS) is usually taken as the position reference. Under the assistance of two intermittent or short continuous external yaw and position, this paper proposed the two-point and the optimum system reset schemes. The proposed system reset schemes are designed based on the $\boldsymbol{P}$ equation and $\boldsymbol{\psi}$ equation. In this paper, the $\boldsymbol{P}$ equation, which relates the position errors to the vector angle $\boldsymbol{\psi}$ and grid yaw error, is reformulated by reserving the horizontal attitude errors as the correction terms in $\boldsymbol{P}$ equation, and the $\boldsymbol{\psi}$ equation which relates the vector angle $\boldsymbol{\psi}$ to the gyroscope drifts is introduced.

### 3.1. The derivation of the modified *P* equation

In order to eliminate the approximate error caused by ignoring the horizontal attitude errors in deriving the $\boldsymbol{P}$ equation, the $\boldsymbol{P}$ equation is reformulated which can be used to design the non-damping system reset algorithm for the SGSINS. In the derivation, $\varphi$ and $\lambda$ denote the latitude and longitude of the ship, and $\rho$ denotes the grid azimuth which is defined as the rotation angle between the grid frame and geographic frame. Accordingly, $\delta\varphi$, $\delta\lambda$ and $\delta\rho$ denote the latitude, longitude and grid azimuth errors. The transformation matrix $\boldsymbol{C}_t^G$ is described as follows:

$$\boldsymbol{C}_t^G = \begin{bmatrix}\cos\rho & -\sin\rho & 0\\ \sin\rho & \cos\rho & 0\\ 0 & 0 & 1\end{bmatrix}. \tag{6}$$

The transformation matrix $\boldsymbol{C}_e^t$ is described as follows:

$$\boldsymbol{C}_e^t = \begin{bmatrix}-\sin\lambda & \cos\lambda & 0\\ -\sin\varphi\cos\lambda & -\sin\varphi\sin\lambda & \cos\varphi\\ \cos\varphi\cos\lambda & \cos\varphi\sin\lambda & \sin\varphi\end{bmatrix}. \tag{7}$$

The computer frame $c$ can be generated by performing three-time rotation of the grid frame $G$ which is illustrated in figure 7.

As shown in figure 7, the frame $Ox'_Gy'_Gz'_G$ is generated by spinning the grid frame around the $x$ axis of the geographic frame by $-\delta\varphi$; the frame $Ox''_Gy''_Gz''_G$ is generated by spinning the frame $Ox'_Gy'_Gz'_G$ around the $z$ axis of the earth-fixed frame

$$Ox_G y_G z_G \xrightarrow[-\delta\varphi]{\text{around } x_t \text{ axis}} Ox_G' y_G' z_G' \xrightarrow[\delta\lambda]{\text{around } z_e \text{ axis}} Ox_G'' y_G'' z_G'' \xrightarrow[-\delta\rho]{\text{around } z_c \text{ axis}} Ox_c y_c z_c$$

**Figure 7.** The transformation from grid frame to computer frame.

by $\delta\lambda$; the computer frame is generated by spinning the frame $Ox_G'' y_G'' z_G''$ around the $z$ axis of the computer frame by $-\delta\rho$. By ignoring the second-order small terms, the projection of $\delta\boldsymbol{\theta}$ on the geographic frame is calculated as follows:

$$\begin{aligned}\delta\boldsymbol{\theta}^t &= \begin{bmatrix}-\delta\varphi\\0\\0\end{bmatrix} \\ &+ \begin{bmatrix}-\sin\lambda & \cos\lambda & 0\\ -\sin\varphi\cos\lambda & -\sin\varphi\sin\lambda & \cos\varphi\\ \cos\varphi\cos\lambda & \cos\varphi\sin\lambda & \sin\varphi\end{bmatrix}\begin{bmatrix}0\\0\\\delta\lambda\end{bmatrix} \\ &+ \begin{bmatrix}1 & \delta\theta_z^t & -\delta\theta_y^t\\ -\delta\theta_z^t & 1 & \delta\theta_x^t\\ \delta\theta_y^t & -\delta\theta_x^t & 1\end{bmatrix}\begin{bmatrix}0\\0\\-\delta\rho\end{bmatrix} \\ &\approx \begin{bmatrix}-\delta\varphi\\ \delta\lambda\cos\varphi\\ \delta\lambda\sin\varphi-\delta\rho\end{bmatrix}. \end{aligned} \tag{8}$$

The projection of $\delta\boldsymbol{\theta}$ on the grid frame is calculated as follows:

$$\begin{aligned}\delta\boldsymbol{\theta}^G &= \boldsymbol{C}_t^G\delta\boldsymbol{\theta}^t \\ &= \begin{bmatrix}\cos\rho & -\sin\rho & 0\\ \sin\rho & \cos\rho & 0\\ 0 & 0 & 1\end{bmatrix}\begin{bmatrix}-\delta\varphi\\ \delta\lambda\cos\varphi\\ \delta\lambda\sin\varphi-\delta\rho\end{bmatrix}. \end{aligned} \tag{9}$$

The components of $\delta\boldsymbol{\theta}^G$ are expressed as follows:

$$\delta\theta_x^G = -\delta\varphi\cos\rho - \delta\lambda\cos\varphi\sin\rho, \tag{10a}$$

$$\delta\theta_y^G = -\delta\varphi\sin\rho + \delta\lambda\cos\varphi\cos\rho, \tag{10b}$$

$$\delta\theta_z^G = \delta\lambda\sin\varphi - \delta\rho. \tag{10c}$$

In the previous research, with the purpose of simplifying the derivation of the $\boldsymbol{P}$ equation, the horizontal attitude errors $\phi_x^G$ and $\phi_y^G$ are approximately zero, and SINS is required to work in damping state to restrain the horizontal attitude errors. In this way, according to (1) and (10), we can obtain the following approximate relationship [17]:

$$\psi_x^G \approx \delta\varphi\cos\rho + \delta\lambda\cos\varphi\sin\rho, \tag{11a}$$

$$\psi_y^G \approx \delta\varphi\sin\rho - \delta\lambda\cos\varphi\cos\rho, \tag{11b}$$

$$\phi_z^G = \delta\lambda\sin\varphi - \delta\rho + \psi_z^G. \tag{11c}$$

The existing $\boldsymbol{P}$ equation is derived based on the approximate relationship in (11), and the system reset algorithms designed based on the existing $\boldsymbol{P}$ equation need to be realized in damping state. The damping of the SINS is usually realized with the aid of DVLs; however, the accuracy of DVLs is extremely vulnerable to the ocean current and maneuvering of the ship. The working state of the SINS frequently switches between the non-damping state and damping state based on the availability of DVLs. In this way, when the working state of the SGSINS switches in the system reset, the error propagation rule of damping SINS breaks, and the estimation accuracy of gyroscope drifts degrades.

This paper proposes a non-damping system reset algorithm which aims to reduce the time using DVL as well as eliminate the approximate error caused by ignoring the horizontal attitude errors. Employing (1) and (10), we can obtain the following equation:

$$\psi_x^G - \phi_x^G = \delta\varphi\cos\rho + \delta\lambda\cos\varphi\sin\rho, \tag{12a}$$

$$\psi_y^G - \phi_y^G = \delta\varphi\sin\rho - \delta\lambda\cos\varphi\cos\rho, \tag{12b}$$

$$\phi_z^G = \delta\lambda\sin\varphi - \delta\rho + \psi_z^G. \tag{12c}$$

We assume the earth is a standard sphere for the purpose of simplifying the derivation, and the radius of the earth $R = 6378393.0$ m. Suppose that the position in the earth-fixed frame is defined as $\begin{bmatrix}x & y & z\end{bmatrix}^{\mathrm{T}}$, then the transformations between $\begin{bmatrix}x & y & z\end{bmatrix}^{\mathrm{T}}$ and $\begin{bmatrix}\lambda & \varphi\end{bmatrix}^{\mathrm{T}}$ are given by

$$\sin\varphi = \frac{z}{R}, \tag{13a}$$

$$\cos\varphi = \frac{\sqrt{x^2+y^2}}{R}, \tag{13b}$$

$$\sin\lambda = \frac{y}{\sqrt{x^2+y^2}}, \tag{13c}$$

$$\cos\lambda = \frac{x}{\sqrt{x^2+y^2}} \tag{13d}$$

where $R$ denotes the earth radius.

By calculating the derivatives on both sides of (13*b*) and (13*c*), $\delta\varphi$ and $\delta\lambda$ can be described as follows:

$$\delta\varphi = -\frac{x\delta x + y\delta y}{z\sqrt{x^2+y^2}}, \tag{14a}$$

$$\delta\lambda = \frac{x\delta y - y\delta x}{x^2+y^2}. \tag{14b}$$

The transformations between grid azimuth $\rho$ and $\begin{bmatrix}\lambda & \varphi\end{bmatrix}^{\mathrm{T}}$ are given by

$$\sin\rho = \frac{\sin\varphi\sin\lambda}{\sqrt{1-\sin^2\lambda\cos^2\varphi}}, \tag{15a}$$

$$\cos\rho = \frac{\cos\lambda}{\sqrt{1-\sin^2\lambda\cos^2\varphi}}. \tag{15b}$$

Using (13) in (15) yields

$$\sin\rho = \frac{yz}{\sqrt{x^2+y^2}\sqrt{x^2+z^2}}, \tag{16a}$$

$$\cos\rho = \frac{Rx}{\sqrt{x^2+y^2}\sqrt{x^2+z^2}}. \tag{16b}$$

Using (13), (14) and (16) in (12) yields

$$\psi_x^G - \phi_x^G = -\frac{\sqrt{x^2+z^2}}{Rz}\delta x - \frac{xy}{Rz\sqrt{x^2+z^2}}\delta y, \tag{17a}$$

$$\psi_y^G - \phi_y^G = -\frac{1}{\sqrt{x^2+z^2}}\delta y, \tag{17b}$$

$$\phi_z^G = \psi_z^G + \frac{xz\delta y - yz\delta x}{R(x^2+y^2)} - \delta\rho. \tag{17c}$$

Employing (17*a*) and (17*b*), $\delta x$ and $\delta y$ can be described as

$$\delta x = \frac{xy(\psi_y^G - \phi_y^G) - Rz(\psi_x^G - \phi_x^G)}{\sqrt{x^2+z^2}}, \tag{18a}$$

$$\delta y = -\sqrt{x^2+z^2}(\psi_y^G - \phi_y^G). \tag{18b}$$

Using (18) in (14) yields

$$\delta\lambda = \frac{Ryz(\psi_x^G - \phi_x^G) - R^2x(\psi_y^G - \phi_y^G)}{(x^2+y^2)\sqrt{x^2+z^2}}, \tag{19a}$$

$$\delta\varphi = \frac{Rxz(\psi_x^G - \phi_x^G) + yz^2(\psi_y^G - \phi_y^G)}{R\sqrt{x^2+y^2}\sqrt{x^2+z^2}}. \tag{19b}$$

By calculating the derivatives on both sides of (15*b*), $\delta\rho$ can be expressed as follows:

$$\delta\rho = \frac{\delta\lambda\sin\varphi}{1-\sin^2\lambda\cos^2\varphi} + \frac{\delta\varphi\sin\lambda\cos\lambda\cos\varphi}{1-\sin^2\lambda\cos^2\varphi}. \tag{20}$$

Using (13) and (19) in (20) yields

$$\delta\rho = \frac{R^2y(\psi_x^G - \phi_x^G) - Rxz(\psi_y^G - \phi_y^G)}{(x^2+y^2)\sqrt{x^2+z^2}}. \tag{21}$$

Using (18) and (21) in (17*c*) yields

$$\phi_z^G = \psi_z^G - \frac{y}{\sqrt{x^2+z^2}}(\psi_x^G - \phi_x^G). \tag{22}$$

According to (18) and (22), we can obtain the following equation:

$$\begin{aligned}\tilde{\boldsymbol{P}} = \begin{bmatrix}\delta\tilde{x}\\ \delta\tilde{y}\\ \tilde{\phi}_z^G\end{bmatrix} &= \begin{bmatrix}\delta x - \frac{Rz\phi_x^G}{\sqrt{x^2+z^2}} + \frac{xy\phi_y^G}{\sqrt{x^2+z^2}}\\ \delta y - \sqrt{x^2+z^2}\phi_y^G\\ \phi_z^G - \frac{y\phi_x^G}{\sqrt{x^2+z^2}}\end{bmatrix}\\ &= \begin{bmatrix}\frac{-Rz}{\sqrt{x^2+z^2}} & \frac{xy}{\sqrt{x^2+z^2}} & 0\\ 0 & -\sqrt{x^2+z^2} & 0\\ \frac{-y}{\sqrt{x^2+z^2}} & 0 & 1\end{bmatrix}\begin{bmatrix}\psi_x^G\\ \psi_y^G\\ \psi_z^G\end{bmatrix}\\ &= \boldsymbol{M}_G\begin{bmatrix}\psi_x^G\\ \psi_y^G\\ \psi_z^G\end{bmatrix}.\end{aligned} \tag{23}$$

In (23), the modified position errors are related to the vector angle $\boldsymbol{\psi}$ and modified grid yaw error, and (23) is the so-called $\boldsymbol{P}$ equation. Different from the $\boldsymbol{P}$ equation in [17], (23) reserved the horizontal attitude errors, and the horizontal attitude errors are contained as the correction terms in the position errors and grid yaw error. The horizontal attitude errors are estimated through the integration of SGSINS and DVL, which was introduced in section 2.2. Obviously, as long as horizontal attitude errors can be estimated accurately, the modified $\boldsymbol{P}$ equation can be utilized to design the non-damping system reset scheme.

The *OEPQ* frame is first used as the core coordinate system to design the system reset scheme; however, this kind of scheme needs to be realized with the special constraint: the latitude and attitude of the ship are not allowed to change in the system reset. In order to eliminate the constraint, [14, 16, 17, 20] proposed to substitute the inertial frame for the *OEPQ* frame. Here, we adopted the same method to eliminate the constraint. By expressing the vector angle $\boldsymbol{\psi}$ in the inertial frame, (23) can be further modified as follows:

$$\tilde{\boldsymbol{P}} = \begin{bmatrix}\delta\tilde{x}\\ \delta\tilde{y}\\ \tilde{\phi}_z^G\end{bmatrix} = \boldsymbol{M}_G\boldsymbol{C}_i^G\begin{bmatrix}\psi_x^i\\ \psi_y^i\\ \psi_z^i\end{bmatrix} = \boldsymbol{M}_i\begin{bmatrix}\psi_x^i\\ \psi_y^i\\ \psi_z^i\end{bmatrix} \tag{24}$$

where the transformation matrix $\boldsymbol{C}_i^G$ can be calculated as follows:

$$\boldsymbol{C}_i^G = \boldsymbol{C}_t^G\boldsymbol{C}_e^t\boldsymbol{C}_i^e. \tag{25}$$

In (25), the transformation matrixes $\boldsymbol{C}_i^e$, $\boldsymbol{C}_e^t$ and $\boldsymbol{C}_t^G$ can be calculated as follows:

$$\boldsymbol{C}_i^e = \begin{bmatrix}\cos\Omega t & \sin\Omega t & 0\\ -\sin\Omega t & \cos\Omega t & 0\\ 0 & 0 & 1\end{bmatrix}. \tag{26}$$

$$\boldsymbol{C}_e^t = \begin{bmatrix}\frac{-y}{\sqrt{x^2+y^2}} & \frac{x}{\sqrt{x^2+y^2}} & 0\\ \frac{-xz}{R\sqrt{x^2+y^2}} & \frac{-yz}{R\sqrt{x^2+y^2}} & \frac{\sqrt{x^2+y^2}}{R}\\ \frac{x}{R} & \frac{y}{R} & \frac{z}{R}\end{bmatrix}. \tag{27}$$

$$\boldsymbol{C}_t^G = \begin{bmatrix}\frac{Rx}{\sqrt{x^2+y^2}\sqrt{x^2+z^2}} & \frac{-yz}{\sqrt{x^2+y^2}\sqrt{x^2+z^2}} & 0\\ \frac{yz}{\sqrt{x^2+y^2}\sqrt{x^2+z^2}} & \frac{Rx}{\sqrt{x^2+y^2}\sqrt{x^2+z^2}} & 0\\ 0 & 0 & 1\end{bmatrix} \tag{28}$$

where $t$ denotes the time; $\Omega$ denotes the angular velocity of the earth's rotation.

Using (26), (27) and (28) in (25), (24) can be further expressed as follows:

$$\begin{aligned}\tilde{\boldsymbol{P}} &= \begin{bmatrix}z\sin\Omega t & -z\cos\Omega t & y\\ z\cos\Omega t & z\sin\Omega t & -x\\ \frac{Rx\cos\Omega t}{x^2+z^2} & \frac{Rx\sin\Omega t}{x^2+z^2} & \frac{Rz}{x^2+z^2}\end{bmatrix}\begin{bmatrix}\psi_x^i\\ \psi_y^i\\ \psi_z^i\end{bmatrix}\\ &= \boldsymbol{M}_i\begin{bmatrix}\psi_x^i\\ \psi_y^i\\ \psi_z^i\end{bmatrix}.\end{aligned} \tag{29}$$

Equation (29) is the modified $\boldsymbol{P}$ equation which will be utilized to design the system reset schemes in section 4.

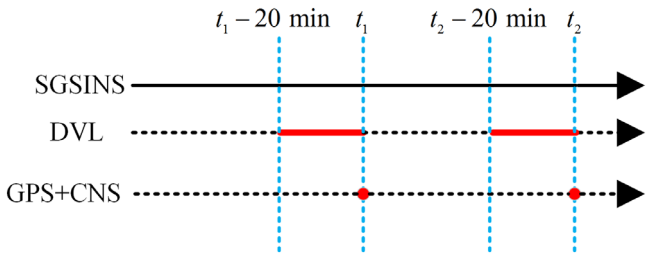


**Figure 8.** The time of introducing DVL, GPS and CNS to the proposed two-point system reset.

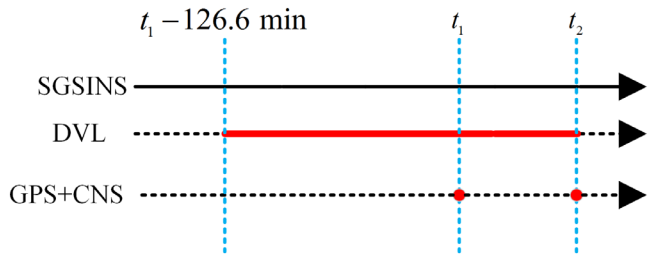


**Figure 9.** The time of introducing DVL, GPS and CNS to the conventional two-point system reset.

### 3.2. The $\psi$ equation

The relationship between the vector angle $\boldsymbol{\psi}$ and gyroscope drifts is formulated as the $\boldsymbol{\psi}$ equation. Similarly, in order to eliminate the constraints of the traditional algorithm on the motion state of the ship, we substituted the inertial frame for the *OEPQ* frame. The $\boldsymbol{\psi}$ equation is expressed as follows [13, 14, 16, 17]:

$$\dot{\boldsymbol{\psi}}^i = \boldsymbol{C}_b^i \boldsymbol{\varepsilon}^b. \tag{30}$$

## 4. The system reset schemes based on external yaw and position

### 4.1. The two-point system reset scheme

Under the assistance of two intermittent external yaw and position, this paper proposes a two-point system reset scheme. Suppose that the SGSINS receives the external yaw and position at time $t_1$ and $t_2$. Since horizontal attitude errors have strong observability, 20 min is enough to obtain accurate estimation results of the horizontal attitude errors. In the two-point system reset scheme, we integrated SGSINS with DVL from $t_1 - 20$ min to $t_1$ and $t_2 - 20$ min to $t_2$, and the estimation results at $t_1$ and $t_2$ are introduced to the system reset. Figure 8 shows the time of introducing DVL, GPS and CNS to the proposed two-point system reset. In figure 8, the red segments indicate the time when the outputs are introduced to the two-point system reset.

Employing (30), the increment of the vector angle $\boldsymbol{\psi}$ from $t_1$ to $t_2$ is described as follows:

$$\Delta\boldsymbol{\psi}_{t_1|t_2} = \boldsymbol{\psi}^i(t_2) - \boldsymbol{\psi}^i(t_1) = \left(\int_{t_1}^{t_2} \boldsymbol{C}_b^i \mathrm{d}t\right) \boldsymbol{\varepsilon}^b. \tag{31}$$

Equation (31) establishes the relationship between the gyroscope drifts and increment of the vector angle. Note that the transformation matrix $\boldsymbol{C}_b^i$ from $t_1$ to $t_2$ is obtained through the recursive calculation of the differential equation $\dot{\boldsymbol{C}}_b^i = \boldsymbol{C}_b^i \boldsymbol{\omega}_{ib}^b \times$ with the gyroscope outputs [14, 16].

Employing (29), the increment of the vector angle $\boldsymbol{\psi}$ from $t_1$ to $t_2$ can be described in another form:

$$\Delta\boldsymbol{\psi}_{t_1|t_2} = \boldsymbol{M}_i^{-1}(t_2)\tilde{\boldsymbol{P}}(t_2) - \boldsymbol{M}_i^{-1}(t_1)\tilde{\boldsymbol{P}}(t_1). \tag{32}$$

At $t_1$, we reset the yaw and position of the SGSINS. Meanwhile, we reset the horizontal attitude according to the estimation results of the horizontal attitude errors from the filter. After the attitude and position reset, $\tilde{\boldsymbol{P}}(t_1) = \boldsymbol{0}$. Then (32) can be further expressed as follows:

$$\Delta\boldsymbol{\psi}_{t_1|t_2} = \boldsymbol{M}_i^{-1}(t_2)\tilde{\boldsymbol{P}}(t_2). \tag{33}$$

At $t_2$, employing (31) and (33), the gyroscope drifts can be calculated as follows:

$$\boldsymbol{\varepsilon}^b = \left(\int_{t_1}^{t_2} \boldsymbol{C}_b^i \mathrm{d}t\right)^{-1} \boldsymbol{M}_i^{-1}(t_2)\tilde{\boldsymbol{P}}(t_2). \tag{34}$$

Equation (34) relates the gyroscope drifts and observation at $t_2$. Obviously, the gyroscope drifts can be estimated under the assistance of two intermittent external yaw and position.

The two-point system reset scheme realized in damping state needs more time to integrate the SGSINS with the DVL. Taking horizontal damping for instance, one and a half periods of Schuler oscillation (84.4 min) are usually required for the process of damping the error into the stable state [26]. In this case, in order to ensure the damping from $t_1$ to $t_2$ reaches the stable state, the integration of SGSINS and DVL should start no later than $t_1 - 1.5 \times 84.4$ min. From the above analysis, the shortest time of using DVL output can be calculated as: $t_2 - t_1 + 126.6$ min. The times of introducing DVL, GPS and CNS to the conventional two-point system reset are shown in figure 9. As shown in figure 8, in the proposed two-point system reset scheme, since the time of using DVL only depends on the time of estimating horizontal attitude errors, we only need to integrate the SGSINS with the DVL for 40 min. In this way, the proposed two-point system reset scheme greatly reduces the time of using DVL output.

### 4.2. The optimum system reset scheme

With the assistance of short continuous external navigation information, the system reset to estimate the gyroscope drifts through the Kalman filter is usually called the optimum system reset. With the assistance of short continuous external yaw and position, this paper proposes an optimum system reset scheme. Suppose that the gyroscope drift consists of constant drift and random drift:

$$\boldsymbol{\varepsilon}^b = \boldsymbol{\varepsilon}_c^b + \boldsymbol{\varepsilon}_r^b \tag{35}$$

where $\dot{\boldsymbol{\varepsilon}}_c^b = \boldsymbol{0}$ represents the gyroscope constant drift; $\boldsymbol{\varepsilon}_r^b$ represents the gyroscope random drift.

By selecting the vector angle $\boldsymbol{\psi}$ and gyroscope constant drift $\boldsymbol{\varepsilon}_c^b$ as the state variables, according to (30) and (35), the

continuous-time linear process equation is formulated as follows:

$$\begin{bmatrix} \dot{\boldsymbol{\psi}}^i \\ \dot{\boldsymbol{\varepsilon}}_c^b \end{bmatrix} = \begin{bmatrix} \mathbf{0}_{3\times3} & \boldsymbol{C}_b^i \\ \mathbf{0}_{3\times3} & \mathbf{0}_{3\times3} \end{bmatrix} \begin{bmatrix} \boldsymbol{\psi}^i \\ \boldsymbol{\varepsilon}_c^b \end{bmatrix} + \begin{bmatrix} \boldsymbol{C}_b^i \boldsymbol{\varepsilon}_r^b \\ \mathbf{0}_{3\times1} \end{bmatrix}. \tag{36}$$

where the transformation matrix $\boldsymbol{C}_b^i$ is calculated as follows:

$$\boldsymbol{C}_b^i = \boldsymbol{C}_e^i \boldsymbol{C}_t^e \boldsymbol{C}_G^t \boldsymbol{C}_b^G. \tag{37}$$

In (37), $\boldsymbol{C}_e^i$ is obtained by calculating the transpose of (26); $\boldsymbol{C}_G^t$ and $\boldsymbol{C}_t^e$ are obtained by calculating the transposes of (28) and (27) with the assistance of the external position. $\boldsymbol{C}_b^G$ is obtained by correcting the attitude errors. Suppose that $\boldsymbol{C}_b^{G'}$ represents the strap-down matrix outputted by the SGSINS, then the strap-down matrix $\boldsymbol{C}_b^G$ can be corrected as follows:

$$\boldsymbol{C}_b^G = \begin{bmatrix} 1 & -\phi_U^G & \phi_N^G \\ \phi_U^G & 1 & -\phi_E^G \\ -\phi_N^G & \phi_E^G & 1 \end{bmatrix} \boldsymbol{C}_b^{G'}. \tag{38}$$

In (38), $\phi_E^G$ and $\phi_N^G$ are estimated by the Kalman filter which has been introduced in section 2.2; $\phi_U^G$ is obtained by calculating the difference between the external yaw and the yaw outputted by the SGSINS. In the proposed optimum system reset scheme, the SGSINS receives the external yaw and position from time $t$ to $t + 10$ min, and the SGSINS is integrated with the DVL from $t - 20$ min to $t + 10$ min. The estimation results of the horizontal attitude errors are introduced to the system reset from $t$ to $t + 10$ min. Figure 10 shows the time of introducing DVL, GPS and CNS to the proposed optimum system reset. In figure 10, the red segments indicate the time when the outputs are introduced to the optimum system reset.

Equation (29) can be rewritten in the following form:

$$\boldsymbol{y}(t) = \boldsymbol{M}_i \boldsymbol{\psi}^i + \boldsymbol{\zeta}(t). \tag{39}$$

where $\boldsymbol{y} = \begin{bmatrix} \delta\tilde{x} & \delta\tilde{y} & \tilde{\phi}_z^G \end{bmatrix}^{\mathrm{T}}$. $\boldsymbol{\zeta}$ represents the measurement noise which includes the measurement noise from GPS and CNS. By selecting the vector angle $\boldsymbol{\psi}$ and gyroscope constant drift $\boldsymbol{\varepsilon}_c^b$ as the state variables, the measurement equation is formulated as follows:

$$\boldsymbol{y}(t) = \begin{bmatrix} \boldsymbol{M}_i & \mathbf{0}_{3\times3} \end{bmatrix} \begin{bmatrix} \boldsymbol{\psi}^i \\ \boldsymbol{\varepsilon}_c^b \end{bmatrix} + \boldsymbol{\zeta}(t). \tag{40}$$

According to (36) and (40), with the assistance of the external yaw and position, the gyroscope constant drifts can be estimated by Kalman filter.

The optimum system reset scheme realized in damping state needs more time to integrate SGSINS with DVL. In order to ensure the damping from $t$ to $t + 10$ min reaches the stable state, the integration of SGSINS and DVL should start no later than $t - 1.5 \times 84.4$ min. From the above analysis, the shortest time of using DVL output is 136.6 min. The time of introducing DVL, GPS and CNS to the conventional optimum system reset are shown in figure 11. As shown in figure 10, in the proposed optimum system reset scheme, since the time of using DVL only depends on the time of estimating horizontal attitude errors, we only need to integrate SGSINS with DVL for 30 min. In this way, the proposed optimum system reset scheme greatly reduces the time of using DVL output.

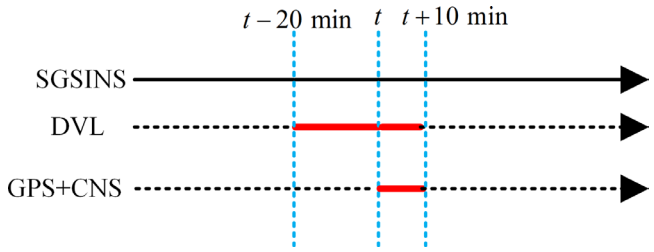


**Figure 10.** The time of introducing DVL, GPS and CNS to the proposed optimum system reset.

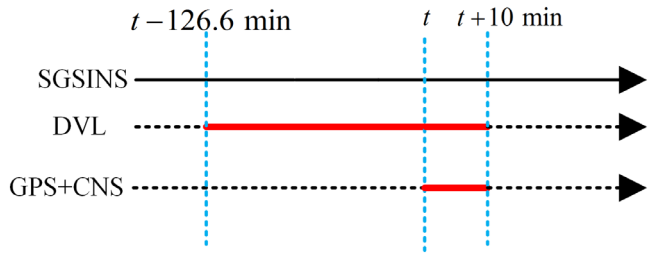


**Figure 11.** The time of introducing DVL, GPS and CNS to the conventional optimum system reset.

**Table 1.** The simulation parameters.

| Parameters | Values |
|---|---|
| Navigation time | 25 h |
| Gyroscope constant drift | $0.01°\ \mathrm{h}^{-1}$ |
| Gyroscope random drift | White noise |
| Accelerometer constant bias | $10^{-4}$ g |
| Accelerometer random bias | White noise |
| Standard deviation of external position error | 10 m |
| Standard deviation of external yaw error | 10″ |
| Initial attitude errors | 6″ 6″ 6′ |
| Initial latitude and longitude | 85°N 18°E |
| Speed of ship | $10\ \mathrm{m\ s}^{-1}$ |
| Attitude change of ship | Sine function |

## 5. Simulation results and analysis

Due to the limitations of performing the experiment in the polar region, we performed a numerical simulation to test the proposed two-point and optimum system reset schemes. The outputs of the gyroscope and accelerometer are generated by an SINS simulator. The simulation parameters are set as in table 1.

The Kalman filter in section 2.2 is utilized to estimate the horizontal attitude errors. The initial state vector $\boldsymbol{x}_0$, estimation error covariance matrix $\boldsymbol{P}_0$, process noise covariance matrix $\boldsymbol{Q}_0$ and measurement noise covariance matrix $\boldsymbol{R}_0$ are initialized as follows:

$$\boldsymbol{x}_0 = \begin{bmatrix} 0 & 0 & 0 & 0 & 0 & 0 & 0 & 0 \end{bmatrix}^{\mathrm{T}},$$

**Table 2.** The operations of scheme 1, scheme 2 and scheme 3 at $t_1 = 2\,\text{h}$ and $t_2 = 6\,\text{h}$.

| | Operations |
|---|---|
| Scheme 1 | No operation |
| Scheme 2 | Attitude and position reset at $t_1 = 2\,\text{h}$ and $t_2 = 6\,\text{h}$ |
| Scheme 3 | Attitude and position reset at $t_1 = 2\,\text{h}$ and $t_2 = 6\,\text{h}$; gyroscope drifts compensation at $t_2 = 6\,\text{h}$ |

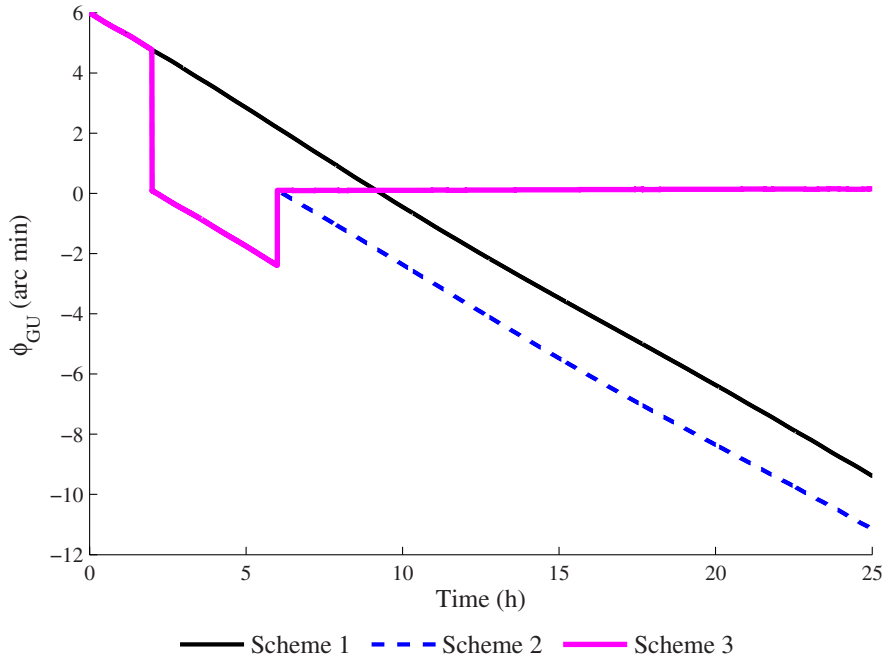


**Figure 12.** The grid yaw error of scheme 1, scheme 2 and scheme 3.

$$\boldsymbol{P}_0 = \text{diag}\{[(6'')^2 \quad (6'')^2 \quad (6')^2 \quad (0.1\ \text{m s}^{-1})^2 \quad (0.1\ \text{m s}^{-1})^2 \quad (5\ \text{m})^2 \quad (5\ \text{m})^2 \quad (5\ \text{m})^2]\},$$

$$\boldsymbol{Q}_0 = \text{diag}\{[(0.01^\circ\ \text{h}^{-1})^2 \quad (0.01^\circ\ \text{h}^{-1})^2 \quad (0.01^\circ\ \text{h}^{-1})^2 \quad (10^{-4}\ \text{g})^2 \quad (10^{-4}\ \text{g})^2]\},$$

$$\boldsymbol{R}_0 = \text{diag}\{[(0.1\ \text{m s}^{-1})^2 \quad (0.1\ \text{m s}^{-1})^2]\}.$$

### *5.1. The simulation results of the two-point system reset scheme*

The ship sails northwards. The SGSINS receives external yaw and position at $t_1 = 2\,\text{h}$ and $t_2 = 6\,\text{h}$. From $t = 1$ h40 min to $t = 2\,\text{h}$ and $t = 5$ h40 min to $t = 6\,\text{h}$, the SGSINS is integrated with the DVL to estimate the horizontal attitude errors. To verify the superiority of the designed two-point system reset scheme, the SGSINS mechanization is tested with different operations at $t_1 = 2\,\text{h}$ and $t_2 = 6\,\text{h}$, named scheme 1, scheme 2 and scheme 3. These are shown in table 2.

Scheme 3 is the proposed two-point system reset scheme. Under the simulation conditions set above, the yaw error and position errors in the earth-fixed frame are drawn in figures 12 and 13.

At $t_2 = 6\,\text{h}$, according to the proposed system reset scheme, the estimated three-axis gyroscope drifts are $0.0092^\circ\ \text{h}^{-1}$, $0.0089^\circ\ \text{h}^{-1}$ and $0.0101^\circ\ \text{h}^{-1}$. Obviously, under the assistance of two intermittent external yaw and position, the two-point system reset scheme can estimate the gyroscope drifts accurately in non-damping state. In theory, compensating the gyroscope drifts can suppress the drifted errors in the SGSINS. The root-mean-squares (RMSs) of position and yaw errors after $t = 6\,\text{h}$ are summarized in table 3.

As shown in figures 12, 13 and table 3, when the SGSINS mechanization is performed without any measure to suppress the errors, the position and yaw errors accumulate rapidly for scheme 1. When the attitude and position reset are operated at $t_1 = 2\,\text{h}$ and $t_2 = 6\,\text{h}$, the position and yaw errors decrease rapidly after the reset at $t_1 = 2\,\text{h}$ and $t_2 = 6\,\text{h}$. However, the navigation errors still accumulate with time as the gyroscope drifts are not compensated in scheme 2. In scheme 3, the accumulated navigation errors have been restrained effectively as the gyroscope drifts are compensated at $t_2 = 6\,\text{h}$. The proposed two-point system reset scheme is performed in non-damping state, and the time of using DVL is only 40 min. However, according to the analysis in section 4.1, the two-point system reset scheme realized in damping needs at least 366.6 min to integrate the SGSINS with the DVL. Therefore, the proposed two-point system reset scheme greatly shortens the time of using DVL, and this improves the reliability of the algorithm in practical application.

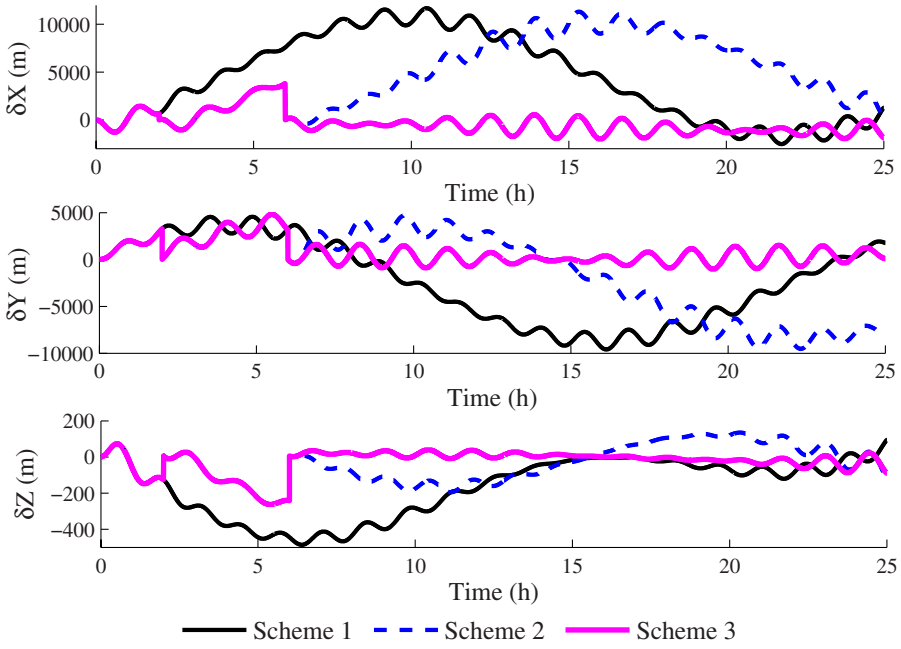


**Figure 13.** The position errors of scheme 1, scheme 2 and scheme 3.

### *5.2. The simulation results of the optimum system reset scheme*

The ship sails northwards. The SGSINS receives external yaw and position from $t = 6\,\text{h}$ to $t = 6\,\text{h}\ 10\,\text{min}$. From $t = 5\,\text{h}\ 40\,\text{min}$ to $t = 6\,\text{h}\ 10\,\text{min}$, the SGSINS is integrated with the DVL to estimate the horizontal attitude errors. Aiming at optimum system reset, the other Kalman filter is utilized to estimate the gyroscope constant drifts, which has been introduced in section 4.2. The initial state vector $\boldsymbol{x}_0'$, estimation error covariance matrix $\boldsymbol{P}_0'$, process noise covariance matrix $\boldsymbol{Q}_0'$ and measurement noise covariance matrix $\boldsymbol{R}_0'$ are initialized as follows:

$$\boldsymbol{x}_0' = \begin{bmatrix} 0 & 0 & 0 & 0 & 0 & 0 \end{bmatrix}^{\mathrm{T}},$$

$$\boldsymbol{P}_0' = \mathrm{diag}\{[(6'')^2 \quad (6'')^2 \quad (6')^2 \quad (0.01^\circ\ \mathrm{h}^{-1})^2 \quad (0.01^\circ\ \mathrm{h}^{-1})^2 \quad (0.01^\circ\ \mathrm{h}^{-1})^2]\},$$

$$\boldsymbol{Q}_0' = \mathrm{diag}\{[(0.001^\circ\ \mathrm{h}^{-1})^2 \quad (0.001^\circ\ \mathrm{h}^{-1})^2 \quad (0.001^\circ\ \mathrm{h}^{-1})^2]\},$$

$$\boldsymbol{R}_0' = \mathrm{diag}\{[(5\mathrm{m})^2 \quad (5\mathrm{m})^2 \quad (10'')^2]\}.$$

To verify the superiority of the designed optimum system reset scheme, the SGSINS mechanization is tested with different operations at $t = 6\,\text{h}\ 10\,\text{min}$, named scheme 1, scheme 2 and scheme 3. These are shown in table 4.

Scheme 3 is the proposed optimum system reset scheme. From $t = 6\,\text{h}$ to $t = 6\,\text{h}\ 10\,\text{min}$, the Kalman filter is utilized to estimate the gyroscope constant drifts based on the state-space model in section 4.2. The estimation results of the gyroscope constant drifts are shown in figure 14.

**Table 3.** The RMSs of position and yaw errors of scheme 1, scheme 2 and scheme 3.

| Navigation errors | Scheme 1 | Scheme 2 | Scheme 3 |
|---|---|---|---|
| Grid yaw error (′) | 0.0825 | 0.1088 | 0.0020 |
| *X*-axis position error (m) | 6728 | 6835 | 995 |
| *Y*-axis position error (m) | 5413 | 5160 | 727 |
| *Z*-axis position error (m) | 210 | 101 | 25 |

As shown in figure 14, the estimation results of the gyroscope constant drifts converge to the stable state in about 200 s. Taking the means of the estimation results from 500 s to 600 s as the estimated gyroscope constant drifts, the estimated gyroscope constant drifts are $0.0090^\circ\,\mathrm{h}^{-1}$, $0.0091^\circ\,\mathrm{h}^{-1}$ and $0.0103^\circ\,\mathrm{h}^{-1}$. Obviously, under the assistance of short continuous external yaw and position, the optimum system reset scheme can estimate the gyroscope constant drifts accurately in non-damping state. Under the simulation conditions set above, the yaw error and position errors in the earth-fixed frame are drawn in figures 15 and 16.

The RMSs of position and yaw errors after $t = 6\,\text{h}\ 10\,\text{min}$ are summarized in table 5.

As shown in figures 15, 16 and table 5, we can find only attitude and position reset at $t = 6\,\text{h}\ 10\,\text{min}$ cannot restrain the errors essentially. The compensation of the gyroscope drifts at $t = 6\,\text{h}\ 10\,\text{min}$ can efficiently improve the navigation accuracy of the SGSINS. The proposed optimum system reset scheme is realized in non-damping state, and the time of using DVL is only 30 min. However, according to the analysis in section 4.2, the optimum system reset scheme realized in damping state needs at least 136.6 min to integrate the SGSINS with the DVL. Therefore, the proposed optimum system reset scheme

**Table 4.** The operations of scheme 1, scheme 2 and scheme 3 at $t = 6\,\text{h}\ 10\,\text{min}$.

| | Operations |
|---|---|
| Scheme 1 | No operation |
| Scheme 2 | Attitude and position reset at $t = 6\,\text{h}\ 10\ \text{min}$ |
| Scheme 3 | Attitude reset, position reset and gyroscope drift compensation at $t = 6\,\text{h}\ 10\ \text{min}$ |

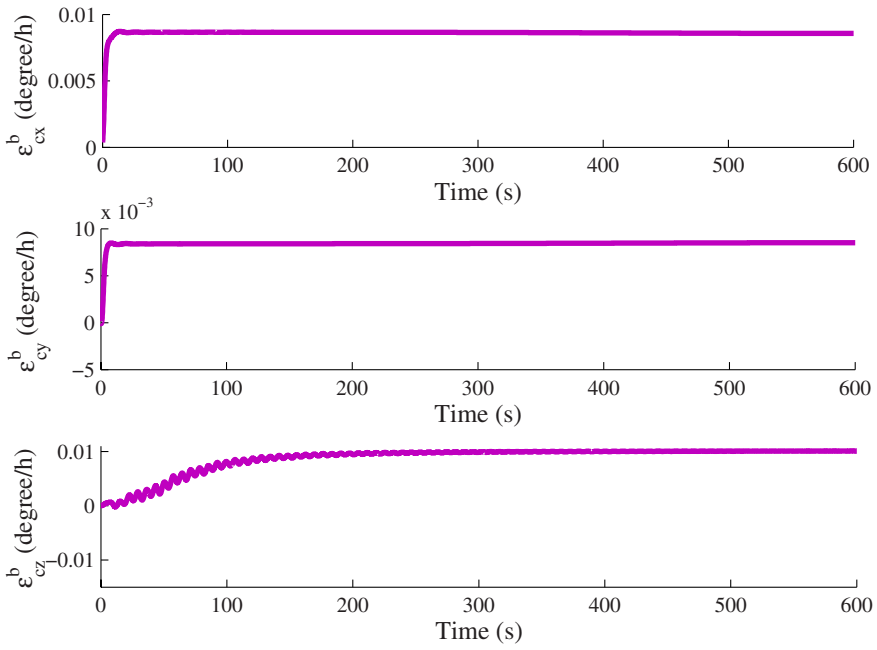


**Figure 14.** The estimation results of the gyroscope constant drifts from $t = 6\,\text{h}$ to $t = 6\,\text{h}\ 10\,\text{min}$.

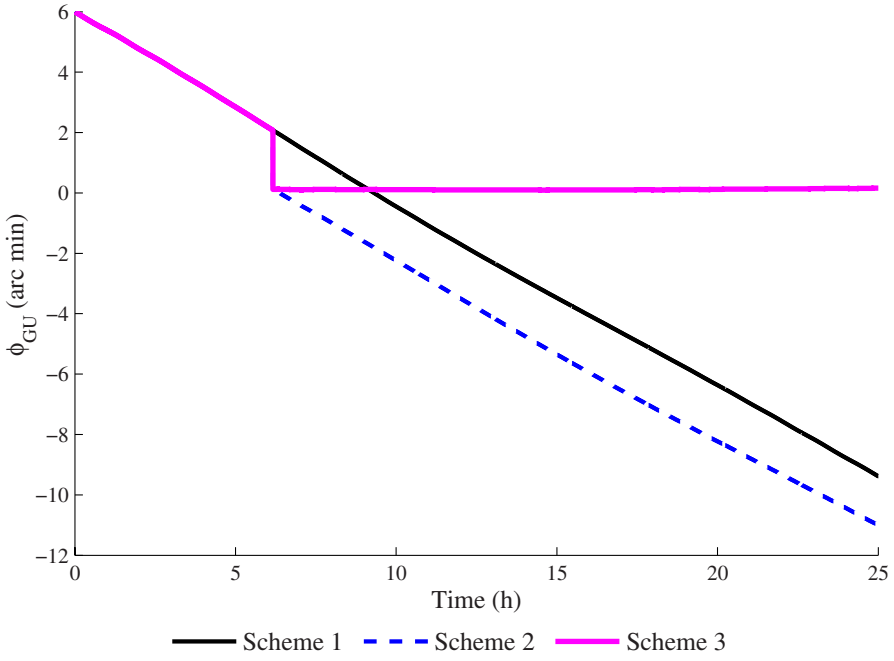


**Figure 15.** The grid yaw error of scheme 1, scheme 2 and scheme 3.

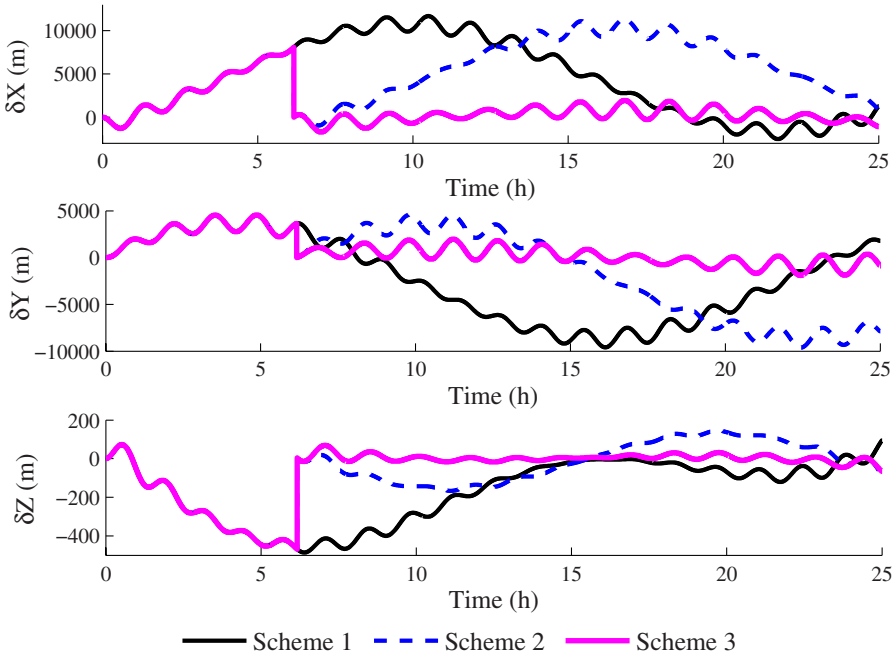


**Figure 16.** The position errors of scheme 1, scheme 2 and scheme 3.

**Table 5.** The RMSs of position and yaw errors of scheme 1, scheme 2 and scheme 3.

| Navigation errors | Scheme 1 | Scheme 2 | Scheme 3 |
|---|---|---|---|
| Grid yaw error ($\iota$) | 0.0828 | 0.1074 | 0.0019 |
| *X*-axis position error (m) | 6718 | 6925 | 786 |
| *Y*-axis position error (m) | 5427 | 5165 | 898 |
| *Z*-axis position error (m) | 206 | 99 | 19 |

reduces the time we depend on DVLs, which has important practical value in engineering.

## 6. Conclusions

In view of keeping the navigation autonomy as well as extending the navigation time of the SGSINS, this paper addressed a non-damping system reset algorithm to estimate the gyroscope drifts. We integrated SGSINS and DVL to estimate the horizontal attitude errors and the estimation results are introduced to the system reset. In order to ensure the system reset algorithm can be realized in non-damping state, the $\boldsymbol{P}$ equation is reformulated by reserving the horizontal attitude errors as the correction terms in the $\boldsymbol{P}$ equation. Under the assistance of two intermittent or short continuous external yaw and position, we designed the two-point and optimum system reset schemes. The numerical simulation indicates the proposed system reset schemes can estimate the gyroscope drifts accurately in non-damping state, and compensating the gyroscope drifts can restrain the drifted errors in the SGSINS. The algorithm greatly reduces the time we depend on DVLs, and this improves the reliability of the algorithm in engineering.

## Acknowledgments

This research was funded by the National Natural Science Foundation of China (Grant Nos. 61773132, 61633008 and 61803115).

## Appendix. The detailed expressions of matrixes $\boldsymbol{C_{AV}}$, $\boldsymbol{C_{AR1}}$, $\boldsymbol{C_{AR2}}$ and $\boldsymbol{C_R}$

$$\boldsymbol{C}_{AV} = \begin{bmatrix} 0 & -\frac{1}{R} & 0 \\ \frac{1}{R} & 0 & 0 \\ 0 & -\frac{\cot\varphi\sin\rho}{R} & 1 \end{bmatrix}, \tag{A.1}$$

$$\boldsymbol{C}_{AR1} = \frac{1}{R^2}\begin{bmatrix} \boldsymbol{C}_1(1,1) & \boldsymbol{C}_1(1,2) & \boldsymbol{C}_1(1,3) \\ \boldsymbol{C}_1(2,1) & \boldsymbol{C}_1(2,2) & \boldsymbol{C}_1(2,3) \\ \boldsymbol{C}_1(3,1) & \boldsymbol{C}_1(3,2) & \boldsymbol{C}_1(3,3) \end{bmatrix} \tag{A.2}$$

where

$$\boldsymbol{C}_1(1,1) = V_N^G\cos\varphi\cos\lambda,$$

$$\boldsymbol{C}_1(1,2) = V_N^G\cos\varphi\sin\lambda,$$

$$\boldsymbol{C}_1(1,3) = V_N^G\sin\varphi,$$

$$\boldsymbol{C}_1(2,1) = -V_E^G\cos\varphi\cos\lambda,$$

$$\boldsymbol{C}_1(2,2) = -V_E^G\cos\varphi\sin\lambda,$$

$$\boldsymbol{C}_1(2,3) = -V_E^G\sin\varphi,$$

$$\boldsymbol{C}_1(3,1) = \frac{2V_N^G \cos^2\varphi \sin\lambda \cos\lambda}{(1-\cos^2\varphi\sin^2\lambda)^{\frac{3}{2}}},$$

$$\boldsymbol{C}_1(3,2) = -V_N^G\sqrt{1-\cos^2\varphi\sin^2\lambda},$$

$$\boldsymbol{C}_1(3,3) = \frac{2V_N^G \sin\varphi\cos\varphi\sin\lambda}{(1-\cos^2\varphi\sin^2\lambda)^{\frac{3}{2}}}$$

where $V_E^G$ and $V_N^G$ denote the grid east velocity and grid north velocity:

$$\boldsymbol{C}_{AR2} = \frac{\Omega}{R(1-\cos^2\varphi\sin^2\lambda)^{\frac{3}{2}}} \begin{bmatrix} \boldsymbol{C}_2(1,1) & \boldsymbol{C}_2(1,2) & \boldsymbol{C}_2(1,3) \\ \boldsymbol{C}_2(2,1) & \boldsymbol{C}_2(2,2) & \boldsymbol{C}_2(2,3) \\ \boldsymbol{C}_2(3,1) & \boldsymbol{C}_2(3,2) & \boldsymbol{C}_2(3,3) \end{bmatrix} \quad \text{(A.3)}$$

where

$$\boldsymbol{C}_2(1,1) = 2\cos^2\varphi\sin\varphi\sin\lambda\cos\lambda,$$

$$\boldsymbol{C}_2(1,2) = -\sin\varphi[\cos^2\lambda + \sin^2\lambda(\sin^2\varphi - \cos^2\varphi)],$$

$$\boldsymbol{C}_2(1,3) = \sin^2\varphi\cos\varphi\sin\lambda,$$

$$\boldsymbol{C}_2(2,1) = \sin^2\varphi,$$

$$\boldsymbol{C}_2(2,2) = 0,$$

$$\boldsymbol{C}_2(2,3) = -\sin\varphi\cos\varphi\cos\lambda,$$

$$\boldsymbol{C}_2(3,1) = -\sin\varphi\cos\varphi\cos\lambda,$$

$$\boldsymbol{C}_2(3,2) = -\sin\varphi\cos\varphi\sin\lambda,$$

$$\boldsymbol{C}_2(3,3) = \cos^2\varphi.$$

$$\boldsymbol{C}_R = \frac{1}{R}\begin{bmatrix} \boldsymbol{C}_R(1,1) & \boldsymbol{C}_R(1,2) & \boldsymbol{C}_R(1,3) \\ \boldsymbol{C}_R(2,1) & \boldsymbol{C}_R(2,2) & \boldsymbol{C}_R(2,3) \\ \boldsymbol{C}_R(3,1) & \boldsymbol{C}_R(3,2) & \boldsymbol{C}_R(3,3) \end{bmatrix} \quad \text{(A.4)}$$

where

$$\boldsymbol{C}_R(1,1) = \frac{\sin\varphi}{\sqrt{1-\cos^2\varphi\sin^2\lambda}},$$

$$\boldsymbol{C}_R(1,2) = 0,$$

$$\boldsymbol{C}_R(1,3) = \frac{-\cos\lambda\cos\varphi}{\sqrt{1-\cos^2\varphi\sin^2\lambda}},$$

$$\boldsymbol{C}_R(2,1) = \frac{\sin\lambda\cos\lambda\cos^2\varphi}{\sqrt{1-\cos^2\varphi\sin^2\lambda}},$$

$$\boldsymbol{C}_R(2,2) = \sqrt{1-\cos^2\varphi\sin^2\lambda},$$

$$\boldsymbol{C}_R(2,3) = \frac{-\sin\lambda\sin\varphi\cos\varphi}{\sqrt{1-\cos^2\varphi\sin^2\lambda}},$$

$$\boldsymbol{C}_R(3,1) = \frac{\cos\varphi\sin\varphi\sin\lambda}{1-\cos^2\varphi\sin^2\lambda},$$

$$\boldsymbol{C}_R(3,2) = 0,$$

$$\boldsymbol{C}_R(3,3) = \frac{-\cos^2\varphi\sin\lambda\cos\lambda}{1-\cos^2\varphi\sin^2\lambda}.$$

## ORCID iDs

Tao Fang https://orcid.org/0000-0003-4114-8637
Weiquan Huang https://orcid.org/0000-0002-3780-9343

## References

[1] Noureldin A, El-Shafie A and Bayoumi M 2011 GPS/INS integration utilizing dynamic neural networks for vehicular navigation *Inf. Fusion* **12** 48–57
[2] Noureldin A, Karamat T B, Eberts M D and El-Shafie A 2009 Performance enhancement of MEMS-based INS/GPS integration for low-cost navigation applications *IEEE Trans. Veh. Technol.* **58** 1077–96
[3] Jurado J, Kabban C M S and Raquet J 2018 A regression-based methodology to improve estimation of inertial sensor errors using Allan variance data *Navigation* **60** 251–63
[4] Kendall E C 1956 Gyro/Grid navigation *J. Navig.* **9** 429–35
[5] Lyon W K 1984 The navigation of arctic polar submarines *J. Navig.* **37** 155–79
[6] Fang T, Huang W Q and Luo L 2019 Damping rotating grid SINS based on a Kalman filter for shipborne application *IEEE Access* **7** 14859–70
[7] Yan Z P, Wang L, Zhang W, Zhou J J and Wang M 2017 Polar grid navigation algorithm for unmanned underwater vehicles *Sensors* **17** 1599
[8] Groves P D 2013 *Principles of GNSS, Inertial, and Multisensor Integrated Navigation Systems* (Boston, MA: Artech House) pp 20–35
[9] Crassidis J L 2006 Sigma-point Kalman filtering for integrated GPS and inertial navigation *IEEE Trans. Aerosp. Electron. Syst.* **42** 750–6
[10] Benso W E and Duplessis R M 1963 Effect of shipboard inertial navigation system position and azimuth errors on sea-launched missile radial miss *IEEE Trans. Mil. Electron.* **MIL-7** 45–56
[11] Bona B E and Smay R J 1966 Optimum reset of ships inertial navigation system *IEEE Trans. Aerosp. Electron. Syst.* **AES-2** 409–14
[12] Yang X D, Shi W M, Xia W X and Cheng J H 2014 *Principle and Application of Semi-Analytical Shipborne Inertial Navigation* (China: National Defence Industrial Press) pp 175–89
[13] Zhang X 2014 A novel comprehensive calibration method for long-endurance strapdown inertial navigation system *Ship Electron. Eng.* **34** 47–51
[14] Gao W, Shi H Y, Zhang X and Yang J 2014 Comprehensive correction technology of strapdown inertial navigation system based on position information *J. Huazhong Univ. Sci. Technol.* **42** 101–6 (Natural Science Edition)

[15] Li K, Wang W, Liu F and Zhang J J 2012 New comprehensive damping and correction algorithm for long-endurance inertial navigation system *Chin. J. Sci. Instrum.* **33** 543–8
[16] Li Q, Ben Y Y, Yu F and Sun F 2015 System reset of transversal strapdown INS for ship in polar region *Measurement* **60** 247–57
[17] Huang W Q, Fang T, Lynch A F and Wang Z Y 2019 Comprehensive calibration algorithm for long-endurance shipborne grid SINS *Meas. Sci. Technol.* **30** 105104
[18] Xia W X, Yang X D and Wang W 2012 Research on undamped comprehensive calibration of SINS *Shipbuild. China* **53** 100–8
[19] Huang W Q, Fang T, Luo L, Zhao L and Che F Z 2017 A damping grid strapdown inertial navigation system based on a Kalman filter for ships in polar regions *Sensors* **17** 1551
[20] Feng L, Deng Z H, Wang B and Wang S T 2016 A one-position comprehensive calibration method for long-endurance strapdown inertial navigation systems *Acta Armam.* **37** 265–71
[21] Yu K, Li L, Liu W R and Zhuang L J 2008 Correction of SINS based on undamped navigation mode *J. Chin. Inertial Technol.* **16** 637–42
[22] Hegrenaes Ø and Hallingstad O 2011 Model-aided INS with sea current estimation for robust underwater navigation *IEEE J. Ocean. Eng.* **36** 316–37
[23] Jalving B, Gade K, Svartveit K, Willumsen A and Sorhagen R 2004 DVL velocity aiding in the HUGIN 1000 integrated inertial navigation system *Model. Identif. Control* **25** 223–35
[24] Augenstein S and Rock S 2008 Estimating inertial position and current in the midwater *OCEANS 2008 (Quebec City, QC, 15–18 September 2008)* (IEEE)
[25] Xu B, Wang G Y and Bai J L 2017 Optimal design of damping network based on DVL velocity and IMU *Ocean Eng.* **132** 101–13
[26] Zhao L, Li J S, Cheng J H and Hao Y 2016 Damping strapdown inertial navigation system based on a Kalman flter *Meas. Sci. Technol.* **27** 115102